Journal of Building Engineering 121 (2026) 115725

Contents lists available at ScienceDirect

Journal of Building Engineering

journal homepage: www.elsevier.com/locate/jobe

Cement nanocomposite with $CoFe_2O_4$ nanoparticles and graphite flakes for microwave absorption in X-band frequency

Vanamoorthy Mariappan [a], Eliška Křivánková [b], Milan Masař [a], Marek Jurča [a], Michal Machovský [a], Lukáš Kalina [c], Jarmila Vilčáková [a], Ivo Kuřitka [a], Martin Boháč [b], Raghvendra Singh Yadav [a,*]

[a] Centre of Polymer Systems, University Institute, Tomas Bata University in Zlin, Trida Tomase Bati 5678, 760 01, Zlin, Czech Republic
[b] Research Institute of Building Materials, Hnĕvkovského 30/65, 617 00, Brno, Czech Republic
[c] Metrials Research Centre, Brno University of Technology, 61200, Brno, Czech Republic

ARTICLE INFO

Keywords:
Microwave absorption
Cement-based nanocomposites
Graphite
$CoFe_2O_4$ nanoparticles
Impedance matching
Reflection loss

ABSTRACT

This study reports the microwave absorption in cementitious composites through the incorporation of graphite flakes (GF) and ultrasonically synthesized spherical cobalt ferrite ($CoFe_2O_4$) nanoparticles (CF). Composites with 2.5 wt% GF and 7.5 wt% CF were prepared and characterized for their structural, magnetic, mechanical, and electromagnetic properties. The phase purity of CF nanoparticles and the presence of fillers in the cement matrix were confirmed by X-ray diffraction (XRD). The morphology, distribution, and interfacial interactions between the fillers and the cement matrix were examined using field emission scanning electron microscopy (FESEM), energy dispersive X-ray spectroscopy (EDS), and X-ray photoelectron spectroscopy (XPS). Magnetic hysteresis loops revealed a saturation magnetization of 5.8 emu/g for the cement nanocomposite, confirming the retention of some magnetic behaviour of CF in cement matrix. The results demonstrated excellent microwave absorption performance in X-band range, with a minimum reflection loss (RL_{min}) of −41.9 dB at 10.59 GHz and an effective absorption bandwidth (EAB) of 2.4 GHz (below −10 dB) at a thickness of only 2 mm, corresponding to microwave absorption efficiency of 99.994%. The obtained microwave absorption performance is attributed to the synergistic effects of permittivity and permeability, favourable impedance matching, and high attenuation constant due to the combined dielectric loss from GF and magnetic loss from CF. Despite a slight reduction in mechanical strength compared to the reference, the composite meets standard structural requirements. This work highlights the potential of using conductive and magnetic nanofillers to develop high-performance cementitious composites for X-band microwave absorption applications.

1. Introduction

Electromagnetic (EM) wave radiation has become a significant environmental concern, especially with the rapid spread of electronic devices and communication technologies. Developing efficient EM wave absorbers is critical not only for reducing health risks associated with prolonged exposure to EM radiation but also for protecting vital infrastructure from radar detection and ensuring the

* Corresponding author.
E-mail address: yadav@utb.cz (R.S. Yadav).

https://doi.org/10.1016/j.jobe.2026.115725
Received 23 September 2025; Received in revised form 7 January 2026; Accepted 25 February 2026
Available online 26 February 2026
2352-7102/© 2026 The Authors. Published by Elsevier Ltd. This is an open access article under the CC BY license (http://creativecommons.org/licenses/by/4.0/).

proper functioning of sensitive electronic equipment, such as in defense and hospital buildings [1–4]. Consequently, there is an urgent need for cost-effective and scalable EM wave absorption solutions, particularly in the construction industry, where materials like cement composites are widely used.

The concept of multifunctionality in cement-based composites extends beyond their conventional structural roles. These materials are now being engineered to exhibit additional functionalities such as self-sensing, self-healing, and EM wave absorption [5–9]. This multifunctionality is primarily achieved by incorporating functional fillers and modifying the composite's microstructure [10–12]. Such advancements have enabled cement-based composites to serve not only as building materials but also as active components in absorption against electromagnetic waves, especially in microwave regions. Cement-based composites have harvested attention as potential microwave absorbers due to their affordability, availability, and mechanical robustness [13,14]. However, the challenge lies in optimizing these composites for microwave absorption without compromising their structural integrity. Traditionally, the amount of microwave absorber materials that can be added to cement composites is limited to maintain workability and mechanical strength [15].

Despite these limitations, recent advances in microwave absorbing cementitious materials increasingly rely on nanostructured dielectric and magnetic fillers to overcome the inherently weak attenuation capacity of plain cement matrices. Dai et al. demonstrated that even unmodified Portland cement exhibits measurable dielectric loss due to residual carbon and iron oxides, achieving a minimum reflection loss (RL) of −17.9 dB at 3.14 GHz with a 5 mm specimen, and effective absorption bandwidths up to 10.74 GHz at increased thicknesses [16]. Wang et al. reported that incorporating reduced graphene oxide (RGO), enhances dielectric polarization and conductive loss, and at 3.0 wt% RGO, the composite achieved an RL_{min} of −48.33 dB at 8.9 GHz with 2.6 mm thickness, and an EAB of 5.02 GHz at 1.6 mm [17]. In magnesium phosphate cement (MPC), Liu et al. showed that synergistic addition of 40 vol% hollow glass microspheres (HGM) and 5 wt% Fe_3O_4@SiO_2 nanoparticles produce a uniform impedance-matched network, yielding a 104% increase in absorption peak compared to Fe_3O_4 alone and an effective absorption bandwidth of 1.20 GHz [18]. Xie et al. showed that combining graphene and Mn–Zn ferrite enables synergistic dielectric–magnetic loss, yielding an RL of −22.13 dB at 3.23 GHz for a 25 mm mortar [19]. Bai et al. reported that graphite-enhanced foam concrete improves pore regulation and conductivity, reaching −24.08 dB at 10 mm [20]. Chen et al. achieved ultrathin, broadband absorption by integrating multi-dimensional carbon materials, obtaining an exceptional RL of −44.32 dB at only 1.9 mm thickness [21]. Wu et al. developed lightweight foamed cement using secondary aluminium ash and carbon black, achieving a wide EAB of 14.46 GHz and a peak RL of −36.34 dB at 4 cm [22].

Furthermore, numerous studies have demonstrated that spinel ferrite nanoparticles, when incorporated into different matrices, serve as highly effective fillers for enhancing microwave absorption [23–27]. Among these, $CoFe_2O_4$ spinel ferrite nanoparticles have emerged as particularly promising due to their unique magnetic–dielectric properties and growing interest among researchers. Montazeri et al. synthesized in-situ $CoFe_2O_4$/CoFe/Ti_3C_2 composites via solution combustion, achieving −13 dB reflection loss at 16.3 GHz and an effective absorption bandwidth (EAB) of 3.2 GHz in the Ku band at only 1 mm thickness [28]. Cui et al. developed OPCS@$CoFe_2O_4$ core–shell composites, which combined conductive porous carbon microspheres with magnetic ferrite shells, achieving a minimum reflection loss of −45.4 dB at 2.3 mm and a broadband EAB of 6.3 GHz [29]. Zhang et al. fabricated $CoFe_2O_4$/residual carbon composites from coal gasification slag, demonstrating −43.9 dB reflection loss at 7.76 GHz at 2.4 mm thickness [30]. In addition, a recent study on $CoFe_2O_4$–NRGO (nitrogen doped reduced graphene oxide) hybrids reported by Anil et al. enhanced X-band absorption with strong impedance matching and reflection loss reaching −48.8 dB at 9.6 GHz with 1.7 mm, while PVDF–$CoFe_2O_4$–MXene polymer composites prepared by Wang et al. demonstrated lightweight flexibility and broadband absorption (−54.5 dB with 2.8 mm), confirming the synergy of magnetic ferrites with conductive 2D fillers [31,32]. Collectively, these advances confirm that $CoFe_2O_4$-based nanostructures, especially when integrated with conductive carbons provide synergistic dielectric–magnetic losses and impedance matching, making them highly promising candidates for incorporation into cementitious matrices to enhance microwave absorption.

While many high-performance microwave absorbers utilize graphene or other advanced carbon nanomaterials, their synthesis is often complex, expensive, and difficult to scale for construction use. In contrast, graphite flakes are commercially available, cost-effective. Therefore, developing a cement-based composite that combines a small amount of commercially available conductive graphite with magnetic nanoparticles offers a practical and economical route to achieve strong microwave absorption within a commercially viable thickness, without relying on costly or hard-to-process carbon nanofillers.

This study pioneers the development of a high-performance X-band microwave absorbing cementitious composite by incorporating ultrasonically synthesized spherical cobalt ferrite ($CoFe_2O_4$, CF) nanoparticles and conductive graphite flakes (GF). Unlike our previous work [33], where conductive and magnetic fillers were incorporated individually into cement matrices, this study introduces a synergistic dual-filler strategy, integrating both functional phases into a single composite to achieve best electromagnetic impedance matching and microwave attenuation in thinner cement-based absorbers. The synergistic integration of these fillers with total 10 wt% (7.5 wt% CF for magnetic loss and 2.5 wt% GF for dielectric loss) was engineered to obtain favourable electromagnetic impedance matching, a critical factor often overlooked in cement-based absorbers. To the best of our knowledge, this constitutes the first report detailing the synergistic effect of CF and GF in a cement matrix for microwave absorption, demonstrating a significant advancement over previously reported cementitious absorbers which often require greater thickness or filler loading. Beyond the microwave absorption performance, a comprehensive analysis of the structural, morphological, magnetic, and mechanical properties provides fundamental insights into the material's multifunctional characteristics, highlighting its potential for practical applications in construction where microwave absorption is paramount.

2. Experimental

2.1. Materials

Cobalt nitrate ($Co(NO_3)_2.6H_2O$) and iron nitrate ($Fe(NO_3)_3.9H_2O$) were the products of Lach-Ner, Czech Republic. Graphite flakes (GF) was purchased from Sigma-Aldrich, Germany. For cement composite preparation, CEM I 42.5R (Mokra-Horakov), defoaming agent (DA) from Master Finish DF 880, polycarboxylate ether (PCE) type superplasticizers (MasterEase 1030), and Ligaphobe N90 (Sigma-Aldrich) were used.

2.2. Synthesis of spherical $CoFe_2O_4$ nanoparticles by sonochemical method

To prepare spinel ferrite $CoFe_2O_4$ nanoparticles, the sonochemical method was used. First, appropriate amounts of $Co(NO_3)_2.6H_2O$ and $Fe(NO_3)_3.9H_2O$ were taken into a 250 mL beaker, mixed with 120 mL DI water, and stirred until the precursors dispersed well. In a separate 100 mL beaker, a solution of NaOH was prepared and added slowly into the above-mentioned solution, accompanied by stirring for a few minutes. Then, the obtained thick solution was exposed to ultrasonic irradiation (ultrasonic homogenizer UZ SONOPULS HD 2070) for 70 min at 80 W power and 20 KHz frequency. Afterward, the precipitates were washed and centrifuged several times with DI water until their pH was neutral. Finally, the synthesized product was dried in an oven for 10 h at 80 °C.

2.3. Preparation of cement composite

The additives polycarboxylate ether superplasticizer (PCE, 0.5 wt%), defoaming agent (DA, 0.2 wt%), and Ligaphobe N90 (0.15 wt %) were first dissolved in water (all percentages relative to total cement weight). Graphite flakes (GF, 2.5 wt% of cement) were then added and stirred until fully wetted, followed by spherical $CoFe_2O_4$ nanoparticles (CF, 7.5 wt% of cement). Cement powder (CEM I 42.5R) was subsequently blended with the filler-containing suspension. The water-to-cement (w/c) ratio was 0.30 for the composites. The ligaphobe facilitated the complete immersion of the hydrophobic graphite platelets in the solution. The total filler loading was fixed as 10 wt% to maintain the mechanical integrity of the prepared cement-based nanocomposites. The mixture was hand-stirred for 3 min to ensure homogeneity. The resulting cement paste was then transferred into silicone molds. Excess air was expelled using a vibrating table, which was operated for approximately 5 min. The brief low-intense vibration period, combined with the high viscosity of the fresh cement paste, prevented sedimentation or segregation of the CF nanoparticles and GF. To ensure a smooth surface and prevent the formation of additional air bubbles, a 0.2 mm thick polyethylene foil was placed over the samples. A plexiglass sheet with a heavy load was then applied to the molds. After curing for 24 h in sufficient air moisture (>95 % RH) to avoid crack formation, the samples were removed from the molds and polished using 4000-grit fine sandpaper and a rubber polisher. Mechanical properties were measured after 2, 7, and 28 days, and microwave absorption studies were performed on 28 days old samples.

2.4. Characterization

The characterization process for the developed microwave absorber materials involves a thorough examination of their structural, morphological, magnetic, and electromagnetic properties. To analyze the crystalline structure and phase composition of the samples, X-ray Diffraction (XRD) was utilized (MiniFlex600, Japan, RIGAKU). The surface topography of individual samples was meticulously examined using a NovaNanoSEM 450 Scanning Electron Microscope (ThermoFisher Scientific, The Netherlands), equipped with an Energy Dispersive X-ray Spectroscope (EDS) octane SSD detector (AMETEC, Inc., The US). For acquiring high-resolution SEM (HR-SEM) images, the through-lens detector (TLD) was employed, while the circular backscattered detector (CBS) was used for material contrast and elemental analysis at accelerating voltages of 5 kV and 15 kV, with working distances of 4 mm and 5 mm, respectively. XPS spectra were examined with an X-ray photoelectron spectroscope using Kratos Analytical Axis Ultra DLD system. Flexural (TIRA Test 2710 UTM) and compressive (FORM + Test 5500-2) strength studies were undertaken to analyze the mechanical properties of the prepared nanocomposite. The magnetic properties were assessed by analyzing magnetic hysteresis curves using Vibrating Sample Magnetometry (VSM, Model 7407, Westerville, OH, USA).

The complex permittivity (ε', ε'') and permeability (μ', μ'') of the cement composites were determined from the scattering parameters, tested within the X-band frequency range (8.2-12.4 GHz) using a vector network analyzer (PNA-L N5230A). Further, calculation algorithms were performed using the Nicolson–Ross–Weir (NRW) algorithm [34,35]. The transmission line theory was used to determine the reflection loss values, as summarized in Equations (1) and (2) [19,36,37]:

$$Z_{in} = Z_o \sqrt{\frac{\mu_r}{\varepsilon_r}} \tanh\left[j\left(\frac{2\pi f d}{c}\right)\sqrt{\mu_r \varepsilon_r}\right] \quad (1)$$

$$RL = 20\log\left|\frac{(Z_{in} - Z_o)}{(Z_{in} + Z_o)}\right| \quad (2)$$

Where, Z_{in} represents the input impedance of the absorber and Z_o is the impedance of free space, f, d and c are the EM wave frequency, thickness of the material and velocity of light, respectively. RL is the reflection loss, ε_r is the relative complex permittivity, and μ_r represents the relative complex permeability. Further, the reflection loss efficiency (%) can be evaluated by using the following

equation (3) as [38]:

$$\text{RL Efficiency} = 100 - \left(\frac{1}{10^{RL/10}}\right) \times 100 \quad (3)$$

3. Results and discussion

3.1. XRD

The X-ray diffraction (XRD) patterns (Fig. 1) provide insight into the crystallographic structures of the individual components and the composite material. The diffraction peaks for graphite flakes (GF) are distinctly observed at 2θ values of approximately 26.5° and 54.7°, corresponding to the (002) and (004) planes, respectively, indicating a highly crystalline nature [39–41]. Whereas the XRD pattern of $CoFe_2O_4$ (CF) shows characteristics peaks at 2θ values of 18.3° (111), 30.2° (220), 35.6° (311), 43.2° (400), 53.6° (422), 57.1° (511), and 62.7° (440), confirming its cubic spinel structure [42–44]. For the cement composite (CEM-GF-CF) containing 7.5% CF and 2.5% GF, additional peaks corresponding to portlandite (P), brownmillerite (B), larnite (L), and calcium silicate (C) are identified (Fig. 1c), matching well with previous reports [45,46]. The presence of graphite flakes is further confirmed by the peaks marked as * (002) and * (004), while the cobalt ferrite phases were not visible due to its relatively poor crystalline nature (FWHM ≈ 0.85°) compared to GF (FWHM ≈ 0.14°). The calculated lattice constants are found to be a = 0.2457 nm & c = 0.6704 nm for GF (using equation, $\frac{1}{d_{hkl}^2} = \frac{4}{3}\left(\frac{h^2+hk+k^2}{a^2}\right) + \frac{l^2}{c^2}$) [47–50], and a = 0.8366 nm for spherical CF nanoparticles (using equation, $a = d_{hkl}\sqrt{h^2+k^2+l^2}$) [51–53].

3.2. VSM

The magnetic hysteresis loops, as presented in (Fig. 2a), reveal the magnetic properties of the composite. The cobalt ferrite (CF) shows a characteristic ferromagnetic behavior with high saturation magnetization (Ms) around 53.7 emu/g. In comparison, the CEM-GF-CF composite exhibits magnetization of around 5.8 emu/g, attributed to the dilution of magnetic cobalt ferrite within the non-magnetic cement matrix. The addition of graphite flakes (GF), which exhibit almost negligible magnetic behavior, further reduces the overall magnetization of the composite. A zoomed-in view of the hysteresis loop at low magnetic fields (Fig. 2b), highlighting the coercivity and retentivity values of the CF spherical nanofiller as 479 Oe, 13.1 emu/g and the cement nanocomposite (CEM-GF-CF) as 336 Oe, 1.4 emu/g, respectively.

3.3. Morphological and elemental analysis

The surface morphology and microstructure of the cement composite were studied using Scanning Electron Microscope, and the results are shown in Fig. 3. The micrographs (Fig. 3a–b) reveal the glassy flake-like structure of the graphite flakes, whereas Fig. 3c–d shows the spherical morphology of the ultrasonically prepared cobalt ferrite nanoparticles. Fig. S1, in the supplementary information demonstrates the distribution of CF and GF within the cement matrix, with a selection of specific areas for elemental analysis.

A high-resolution scanning electron microscope (HR-SEM) coupled with EDS analysis is a powerful technique for examining the chemical and physical interactions within the cement-cobalt ferrite (CF)-graphite flake (GF) composite. Fig. 4a shows a representative

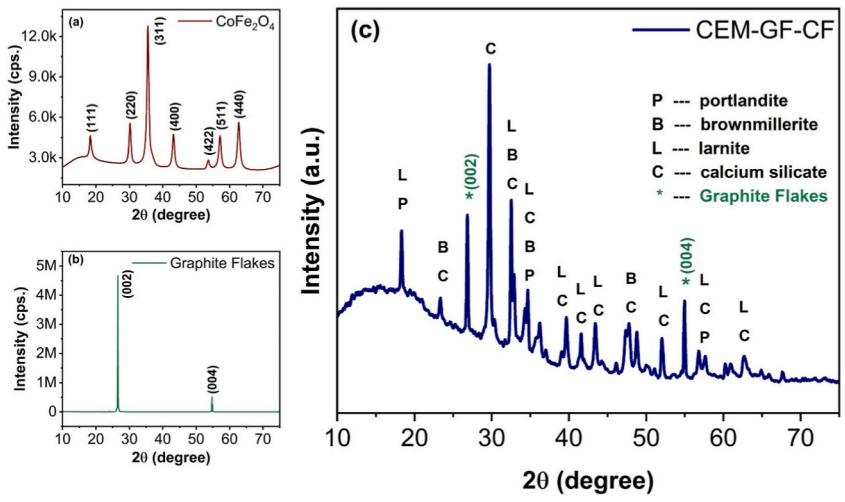

Fig. 1. XRD pattern of **(a)** ultrasonically synthesized spherical $CoFe_2O_4$, **(b)** graphite flakes, and **(c)** CEM-GF-CF composite.

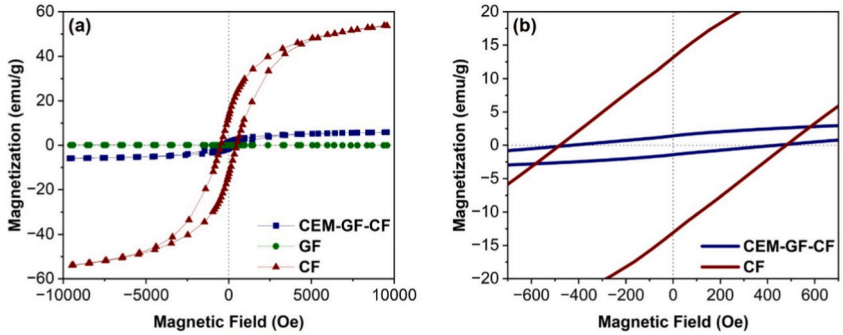

Fig. 2. Magnetic hysteresis loops for **(a)** CF, GF, and CEM-GF-CF composite **(b)** close-up view of the low field region highlighting the coercivity and remanence behavior.

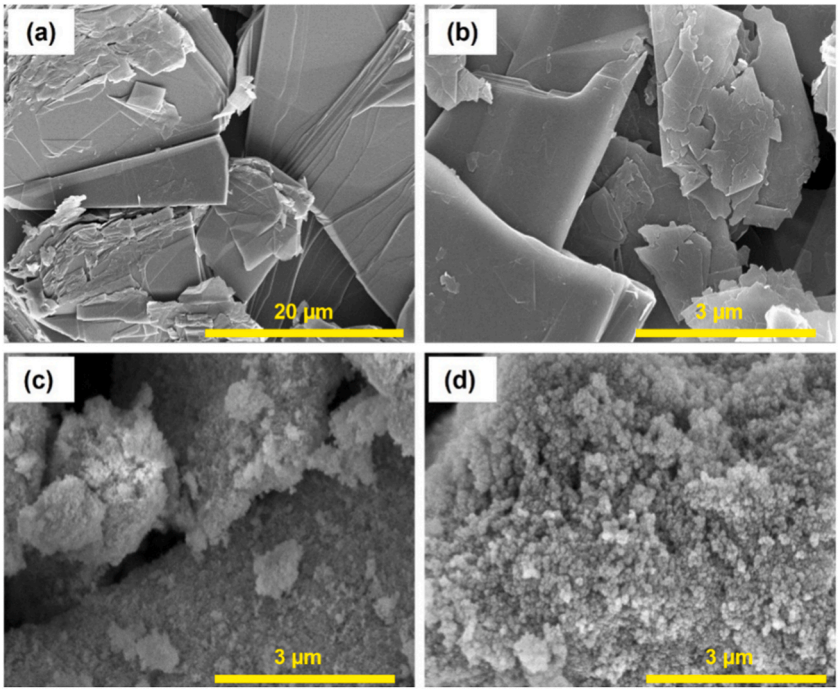

Fig. 3. FE-SEM image of **(a–b)** graphite flakes, and **(c–d)** ultrasonically synthesized spherical CF nanoparticles.

HR-SEM image of the composite, revealing a dense, cohesive microstructure with embedded spherical $CoFe_2O_4$ nanoparticles (bright contrast) and flaky graphite platelets (dark contrast) dispersed in the cementitious matrix. Although some localized agglomeration of fillers is visible, attributed to the hydrophobic nature of graphite and nanoscale magnetic interactions, the overall dispersion supports effective interfacial contact between the fillers and the cement hydration products. Fig. 4b displays the corresponding elemental maps for Ca, Si, O, C, Fe, S, Al, and Co. The uniform distribution of Ca and Si (primary constituents of calcium silicate hydrate, C-S-H) confirms the continuous cementitious binder phase. The maps for Fe and Co (from CF) and C (from GF) illustrate the spatial arrangement of the functional fillers, which is beneficial for combined dielectric and magnetic losses.

Fig. 4c provides a quantitative summary of the elemental composition, highlighting the dominant Ca and Si content alongside measurable contributions from Fe, Co, and C. This microstructural and elemental evidence corroborates the successful incorporation of both conductive and magnetic phases into the cement matrix, forming a heterogeneous but well-integrated composite that facilitates the microwave interactions discussed in subsequent sections. The high calcium and silicon content, primarily from calcium silicate hydrate (C–S–H) and other cement hydration products, forms a continuous binding matrix that mechanically encapsulates and stabilizes the dispersed $CoFe_2O_4$ nanoparticles and graphite flakes, contributing to the composite's structural integrity [54,55]. Some clustering of fillers is observed (Fig. S1), which is attributed to the hydrophobic nature of graphite and nano-scale agglomeration tendencies mentioned earlier.

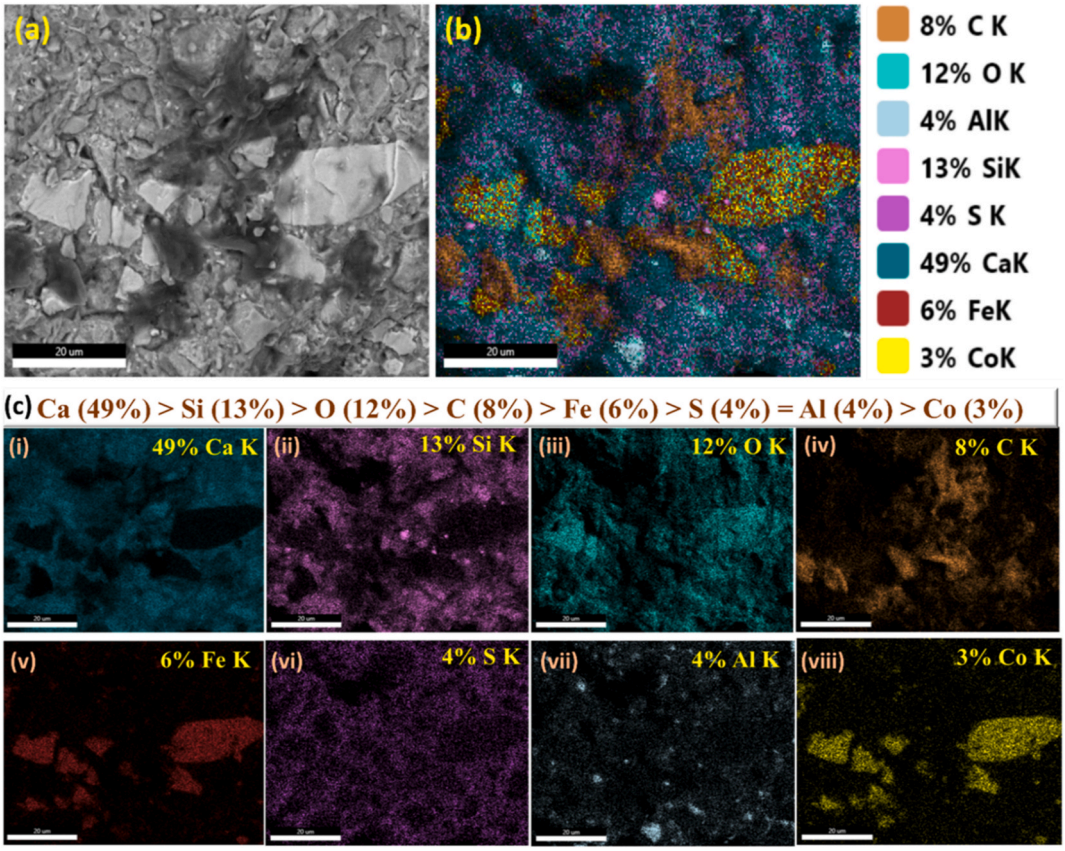

Fig. 4. (a) HR-SEM image, **(b)** elemental mapping, and **(c)** corresponding quantified Ca, Si, O, C, Fe, S, Al, Co maps of CEM-CF-GF nanocomposite.

3.4. XPS

The XPS spectra of Co 2p, Fe 2p, and C 1s were examined and illustrated in Fig. 5 and summarized in Tables 1–2 to understand the surface chemical composition and interaction between the fillers and the cementitious matrix in the composite.

The Co 2p spectrum (Fig. 5a) in cobalt ferrite (CF) shows two main peaks around 780 eV (Co^{2+} in the octahedral (O_h) sites) and 782 eV (Co^{2+} in the tetrahedral (T_h) sites), with a broad satellite feature at higher binding energies [56–58]. In the composite (CEM-CF-GF), the FWHM of these peaks increased from 2.48° to 2.92°, along with a relative increase in the area percentage (61.66% to 69.27%) of Co^{2+} in the octahedral coordination (Fig. 5b). Similarly, the Fe 2p spectrum (Fig. 5c) in pure cobalt ferrite exhibits Fe^{3+} peaks around 710 eV (O_h sites) and 712 eV (T_h sites) [56–58]. Upon incorporation into the composite (Fig. 5d), the FWHM of Fe^{3+} peaks increased from 2.71° to 2.93°, while the relative area percentage of Fe^{3+} in octahedral sites increased from 64.78% to 70.61%. This broadening and redistribution in area percentage imply a change in the local coordination of Co and Fe atoms, possibly due to surface modification or interaction with cement hydration process [56,59,60].

The C 1s spectrum (Fig. 5e) of pure graphite flakes (GF) reveals a dominant C=C peak around 284 eV, with minor components corresponding to C-O-C (286 eV) and C=O (287 eV) functional groups [61,62]. In the composite (Fig. 5f), the C=C peak remains prominent, but there is a notable increase in the C-O-C and C=O peak areas from 4.00% to 13.70% and 1.37% to 5.15%, respectively. This increase suggests the formation of additional oxygen-containing functional groups during the cement hydration process [61,62].

3.5. Mechanical properties

Flexural and compressive studies were undertaken to analyze the mechanical properties of the prepared CEM-CF-GF nanocomposite. The CEM-CF-GF samples (20 × 20 × 100 mm) were prepared and tested for flexural and compressive strengths according to the 196 EN standard in the form of mortar [63]. The results (Fig. 6 & Table 3) show that the addition of 10 wt% fillers (i.e., 2.5 % graphite and 7.5% cobalt ferrite) reduces both flexural and compressive strengths compared to the reference sample. After 28 days, the CEM-GF-CF mix exhibited strengths of 51.89 ± 2.22 MPa (compressive) and 9.92 ± 0.46 MPa (flexural), lower than the reference (64.67 ± 4.38 MPa and 11.32 ± 0.53 MPa). This decline is likely due to graphite's hydrophobic nature, which weakens the interfacial bond with the cement matrix. Additionally, its platy morphology may act as micro-defects, promoting stress concentrations and reducing load-bearing capacity.

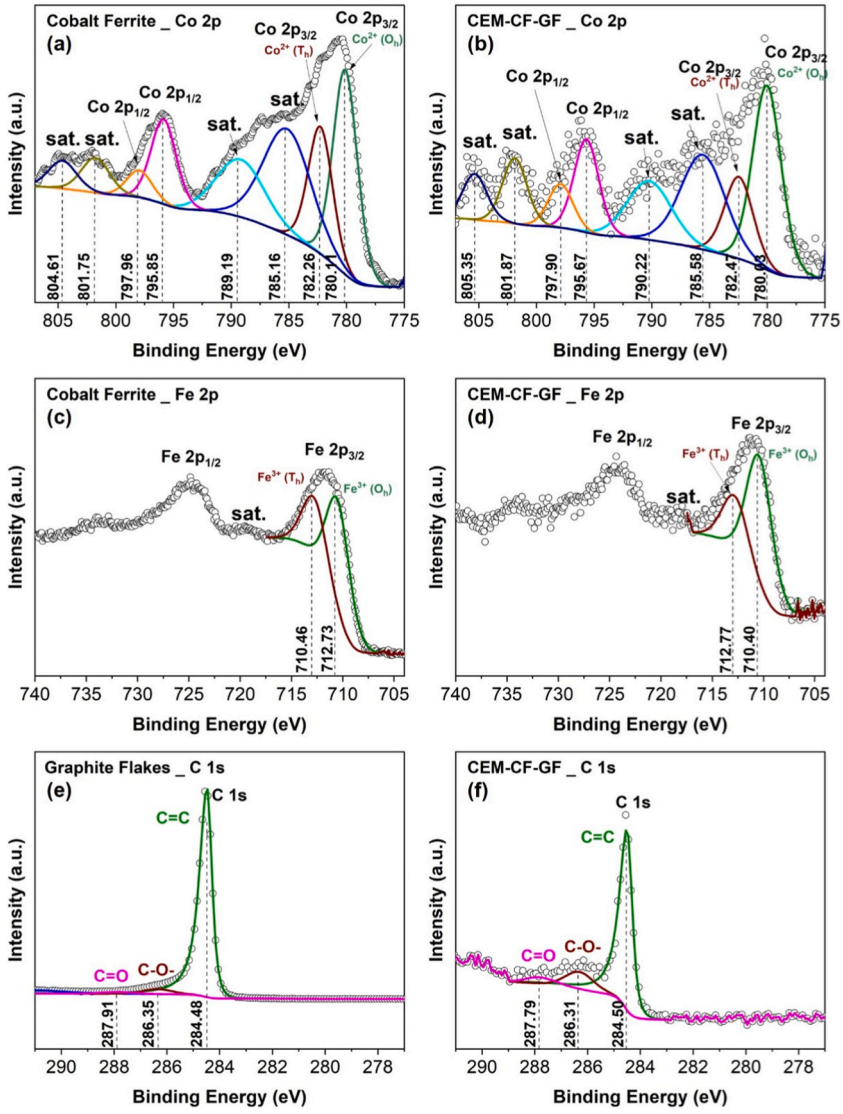

Fig. 5. XPS spectra of **(a–b)** Co 2p, **(c–d)** Fe 2p of pure $CoFe_2O_4$ nanoparticles and CEM-CF-GF nanocomposite, and **(e–f)** C 1s spectra of pure graphite flakes and CEM-CF-GF nanocomposite.

Table 1
Details of Co 2p, Fe 2p spectra of $CoFe_2O_4$ nanoparticles and CEM-CF-GF nanocomposite.

Spectrum	Co $2p_{3/2}$ Co^{2+} (O)		Co $2p_{3/2}$ Co^{2+} (T)		Fe $2p_{3/2}$ Fe^{3+} (O)		Fe $2p_{3/2}$ Fe^{3+} (T)	
Sample	CF	CCG	CF	CCG	CF	CCG	CF	CCG
Binding Energy (eV)	780.11	780.03	782.26	782.47	710.46	710.40	712.73	712.77
FWHM (°)	2.48	2.92	2.48	2.92	2.71	2.93	2.71	2.93
Area (%)	61.66	69.27	38.34	30.73	64.78	70.61	35.22	29.39

Despite the reduction, the CEM-GF-CF composite still meets the EN 197-1 standard for CEM I 42.5R cement, requiring ≥42.5 MPa at 28 days [64]. The slightly higher water-to-cement ratio (0.46 vs. 0.45) suggests that the fillers increase water demand, potentially affecting hydration and microstructure. However, the strength loss is moderate, indicating that the mix remains viable for structural applications where functional properties (e.g., conductivity) are prioritized.

Further improvements could involve optimizing graphite dispersion or surface treatments to enhance compatibility with cement. While the mechanical properties are slightly compromised, the trade-off may be acceptable for specialized applications requiring microwave absorption or electrical conductivity. Future studies could explore hybrid fillers or alternative additives to balance strength

Table 2
Details of C 1s spectra of pure graphite flakes and CEM-CF-GF nanocomposite.

Spectrum	C 1s (C=C)		C 1s (C-O-C)		C 1s (C=O)		
Sample	CF	GF	CCG	GF	CCG	GF	CCG
Binding Energy (eV)	780.11	284.48	284.50	286.35	286.31	287.91	287.79
FWHM (°)	2.48	0.45	0.46	1.32	1.27	1.32	1.27
Area (%)	61.66	89.38	81.14	4.00	13.70	1.37	5.15

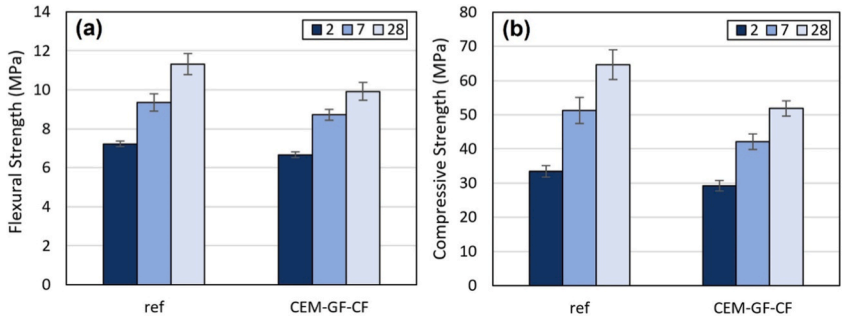

Fig. 6. (a) Flexural and **(b)** compressive strengths of the CEM-CF-GF samples after 2, 7, and 28 days of curing.

Table 3
Flexural and compressive strengths of CEM-CF-GF nanocomposite after 2, 7, and 28 days of curing.

	ref.		CEM-GF-CF	
	Flexural (MPa)	Compressive (MPa)	Flexural (MPa)	Compressive (MPa)
2 days	7.22 ± 0.15	33.39 ± 1.65	6.66 ± 0.15	29.21 ± 1.49
7 days	9.35 ± 0.44	51.27 ± 3.83	8.72 ± 0.28	42.13 ± 2.27
28 days	11.32 ± 0.53	64.67 ± 4.38	9.92 ± 0.46	51.89 ± 2.22

and functionality.

3.6. Microwave absorption properties

The reflection loss (RL) characteristics of the cement composite (CEM-GF-CF) was evaluated over the X-band frequency range (8.2-12.4 GHz). Fig. 7 presents the RL curve for CEM-GF-CF composite sample at 2 mm thickness. As shown, the sample achieved the minimum RL value of −41.9 dB at 10.59 GHz (corresponding to 99.994% microwave absorption). Moreover, an effective absorption

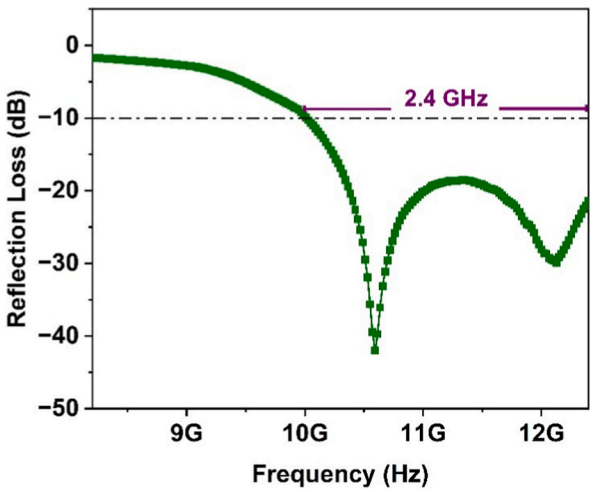

Fig. 7. Reflection loss over frequency of CEM-GF-CF composite at 2 mm thickness.

bandwidth of 2.4 GHz within the frequency range of 10.0-12.4 GHz (RL < −10 dB) was achieved at 2 mm thickness, demonstrating efficient microwave absorption capability. Further, Table 4 compares the microwave absorption properties of the present work with some previously published cement-based composites. Overall, the reflection loss result confirms the potential of CEM-GF-CF composite at 2 mm thickness as an effective X-band microwave absorbing material.

3.7. Electromagnetic parameters

It is well known that the obtained reflection loss value and the microwave absorption performance of any material can be explained by the association between electromagnetic parameters. For that, it is important to analyze the intrinsic parameters such as the material's complex permittivity, permeability, ac conductance, cole-cole plots, eddy current losses, skin depth, attenuation constant, and impedance matching coefficient. These properties, in turn, have a direct impact on the reflection loss values across a range of frequencies, revealing key insights into the material's performance as an effective microwave absorber [68–72]. The complex permittivity (ε_r) and permeability (μ_r), which consists of the real part (ε' and μ') representing the stored energy and the imaginary part (ε'' and μ'') representing the energy loss, given by equations (4) and (5) [73,74].

$$\varepsilon_r = \varepsilon' - j\varepsilon'' \tag{4}$$

$$\mu_r = \mu' - j\mu'' \tag{5}$$

Fig. 8a reveals the real and imaginary part of the permittivity of CEM-GF-CF varies between 11.5-11.9 and 2.2-2.5, respectively. The composite also obtained real permeability between 0.8 and 1.1 and imaginary permeability between 0.0 and 0.26 (Fig. 8b). These obtained values can be attributed to the inclusion of GF and CF in the cement matrix. The ac conductance values, which are directly related to the complex permittivity and the material's conductive pathways, were investigated for the composite CEM-GF-CF with a change in frequency using the following equation [75,76].

$$\sigma_{ac} = \varepsilon_o \varepsilon'' 2\pi f \tag{6}$$

Fig. 9a shows an upward trend of the ac conductivity over the frequency of CEM-GF-CF. The ac conductivity was in the range from 1.0×10^{-2} – 1.7×10^{-2} S/cm [77,78]. The cole-cole plot is a powerful tool for analyzing dielectric relaxation processes in materials, particularly within the context of microwave absorption. These plots allow for a better understanding of how microwave is dissipated through conductivity and polarization mechanisms in a material. The dielectric relaxation process in materials, especially in the GHz frequency range, is vital for evaluating the effectiveness of microwave absorbers. According to Debye's theory, the interaction between the components of complex permittivity can be described by specific mathematical relationships [75,79].

$$\varepsilon' = \varepsilon_\infty + \frac{\varepsilon_s - \varepsilon_\infty}{1 + (\omega\tau)^2}$$

$$\varepsilon'' = \frac{\varepsilon_s - \varepsilon_\infty}{1 + (\omega\tau)^2}\omega\tau + \frac{\sigma}{\omega\varepsilon_o}$$

Where, ε_∞ is the relative dielectric permittivity at an infinitely high frequency, ε_s is the static dielectric permittivity, and symbols ω and τ represent the angular frequency and polarization relaxation time, respectively. From the above equations, the relationship between ε'

Table 4
Microwave absorption characteristics of some cementitious composites containing different types of filler materials.

Filler Material	Filler Amount	Frequency Range (GHz)	RL_{min} (dB)	EAB < −10 dB (GHz)	Thickness (mm)	Ref.
RGO	3 wt%	2-18	−48.3	~2	2.6	[17]
HGM	40 vol%	1-18	−16.2	1.2	20	[18]
Fe_3O_4@SiO_2	5 wt%					
Graphene	0.1 wt%	1-18	−22.13	2.66	25	[19]
MgO	30 wt%					
Graphite	10 wt%	0.2-5	−24.08	0.46	10	[20]
MCS	0.106 wt%	8.2-12.4	−44.32	3.64	1.9	[21]
CNT	1.052 wt%					
Graphene	1.024 wt%					
CB	10 kg/m^3	1.1-18	−36.34	14.46	40	[22]
HGM	10 wt%	8-18	−12.4	5.2	20	[65]
CB	3 wt%					
Mn-Zn Ferrite	25 wt%	0.2-5	−28.7	1.46	10	[66]
Carbon Fibre	0.3 wt%					
CB	2.5 wt%	8-26.5	−20.3	11.6	30	[67]
GF	2.5 wt%	8.2-12.4	−41.9	2.4	2	**This work**
CF	7.5 wt%					

RGO-Reduced Graphene Oxide, HGM-Hollow Glass Microspheres, MCS-Modified Carbon spheres, CNT-Carbon Nanotubes, CB-Carbon Black, GF-Graphite Flakes, CF-$CoFe_2O_4$.

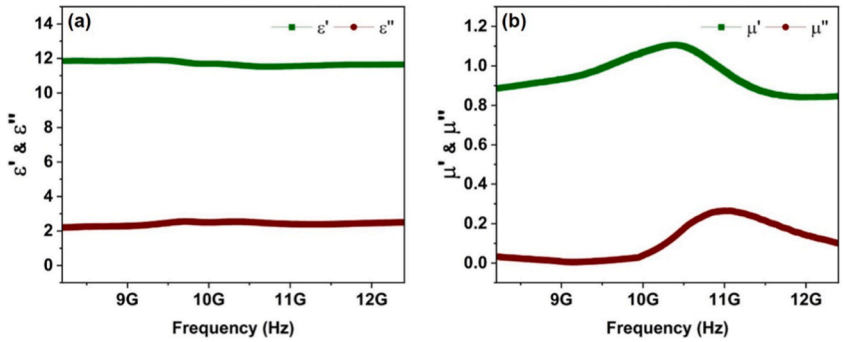

Fig. 8. Variation of **(a)** complex permittivity and **(b)** complex permeability with changing frequency of CEM-GF-CF nanocomposites.

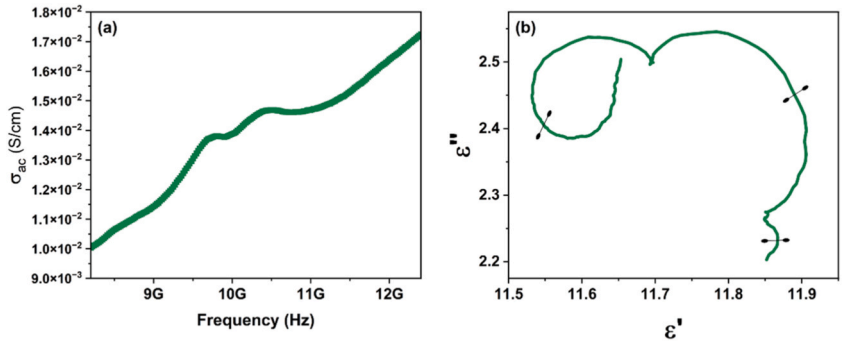

Fig. 9. Variation of **(a)** ac conductivity, and **(b)** cole-cole plot of CEM-GF-CF nanocomposites.

and ε″ can be expressed as [80]:

$$\left(\varepsilon' - \frac{\varepsilon_s + \varepsilon_\infty}{2}\right)^2 + (\varepsilon'')^2 = \left(\frac{\varepsilon_s + \varepsilon_\infty}{2}\right)^2 \tag{7}$$

For an ideal dielectric material following Debye's theory, the relationship between ε′ and ε" would result in a perfect semicircle on the cole-cole plot. However, in real-world materials, deviations from this ideal behavior, such as overlapping or distorted semicircles, indicate the presence of multiple relaxation processes [81–83]. These processes can arise due to the heterogeneous structure of the material, leading to different dipolar and interfacial polarization mechanisms [68].

In the cole-cole plot provided (Fig. 9b), we observe multiple semicircles, suggesting that the material exhibits several dielectric relaxation processes. This behavior is attributed to the heterogeneous nature of the prepared CEM-CF-GF composite, which likely includes a combination of different phases or components that contribute uniquely to the overall dielectric response. This distribution of relaxation times enhances the dielectric loss factor, particularly at lower frequencies, where interfacial polarization is more dominant [84]. Consequently, the broad dispersion in the cole-cole plot supports the observed frequency-dependent behavior of the reflection loss values [71,85].

Further, two other important aspects attributing to the microwave absorption mechanism of a material are the dielectric loss (tan

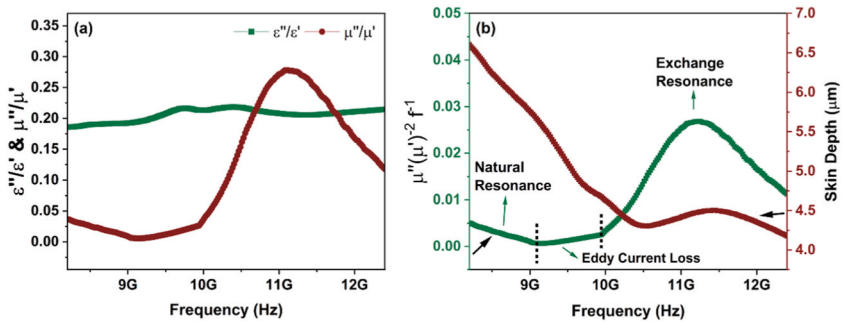

Fig. 10. (a) dielectric loss & magnetic loss tangents, and **(b)** eddy current & skin depth over frequency of CEM-GF-CF nanocomposites.

δ_ε) and magnetic loss (tan δ_μ) [86]. These factors were evaluated using equations (8) and (9), respectively [18,87]:

$$\tan \delta_\varepsilon = \frac{\varepsilon''}{\varepsilon'} \tag{8}$$

$$\tan \delta_\mu = \frac{\mu''}{\mu'} \tag{9}$$

Fig. 10a illustrates the dielectric loss ($\varepsilon''/\varepsilon'$) and magnetic loss ($\mu''/\mu'$) tangents of CEM-GF-CF. The dielectric loss obtained a very minimum fluctuation with value between 0.19 and 0.22, whereas the magnetic loss values vary from 0.0 to 0.28. It is a well-known concept that the values of dielectric loss of a material can be attributed to the stimulus of different kinds of polarizations (dipole, interfacial, electronic, etc.) and conductive loss [88,89]. It is true in this case also that the dipole polarization and the interfacial polarization played a major role, confirmed by the multiple cole-cole semicircle analysis. In addition to this, the presence of effective conductive loss due to the incorporation of GF in the cement matrix, which might have improved the conductive path networks, led to increased electric flow and charge hopping. In the case of magnetic loss, mechanisms such as eddy current loss, hysteresis loss, natural resonance, and exchange resonance have a direct impact on its value [38,90]. Hysteresis loss, which originates from irreversible magnetization processes, is usually negligible in the high-frequency range (e.g., 2-18 GHz). The natural resonance of magnetic nanoparticles and eddy current losses are more relevant at these frequencies. The eddy current coefficient was evaluated using the following equation (10) [72,73] to understand the possible influence of the eddy current on the composite's magnetic loss.

$$C_0 = \mu''(\mu')^{-2} f^{-1} \tag{10}$$

Eddy current losses, which are induced circulating currents within conductive materials exposed to a changing magnetic field, can be confirmed if C_0 remains constant with changing frequency. It is reported that the presence of a peak between 2-10 GHz and 10-18 GHz corresponds to natural resonance and exchange resonance, respectively [82,91]. It can be seen from Fig. 10b, that first there is a decrease in C_0 value from 8.2 to 9.0 GHz, corresponds to the natural magnetic resonance. Then, from 9.0 to 10.0 GHz C_0 remains constant, suggesting that eddy current losses contribute to this trend. The following peak between 10.0 and 12.4 GHz can be attributed to the exchange magnetic resonance behavior of the composite [69,92]. This trend confirms the role of natural resonance, eddy current loss, and exchange resonance in the magnetic loss mechanism.

The skin depth (δ) represents the depth at which electromagnetic waves penetrate the material before being significantly attenuated. It can be calculated using formula (11) [93–95].

$$\delta = \frac{1}{\sqrt{\pi \mu_r \sigma f}} \tag{11}$$

As shown in Fig. 10b, the skin depth for the CEM-CF-GF composite decreases from 4.2 to 6.5 μm with increasing frequency, indicating that higher frequencies lead to greater attenuation of the electromagnetic waves near the material's surface. These losses are more pronounced at higher frequencies due to the skin effect, where the electromagnetic waves are confined to the material's surface, thereby reducing the effective penetration depth or skin depth [70,96,97]. The decreased skin depth with increasing frequency indicates that the material's conductive and magnetic components effectively convert the microwave energy into heat at those frequencies. This phenomenon is directly correlated with the improved attenuation constant, which quantifies the rate of exponential decay of the microwave as it penetrates the composite material.

To understand better the reason behind enhanced reflection loss values at a particular thickness (i.e., 2 mm with the lowest minimum RL of −41.9 dB), the quarter-wavelength matching condition was calculated using equation (12) [58,98,99]:

$$t_m = \frac{nc}{4 f_m \sqrt{|\varepsilon_r||\mu_r|}} \; ; \; n = 1, 3, 5, \tag{12}$$

where n is an odd number (in this case, n = 1), λ is the wavelength in the absorber, c is the speed of light, and μ_r and ε_r are the relative permeability and permittivity of the material. In the given system, the calculated t_m values decrease monotonically with increasing frequency, in accordance with the inverse relation to frequency [100]. In Fig. 11, the variation of the quarter-wavelength matching thickness (t_m) with frequency is plotted alongside the corresponding RL values. It can be observed that the minimum reflection loss of −41.9 dB occurs at around 10.6 GHz, which corresponds closely to a calculated t_m of around 2 mm. Notably, the strongest absorption at this frequency at 2 mm thickness, suggesting that it approaches the ideal quarter-wavelength matching condition. To provide deeper insight into the thickness-dependent absorption behaviour, three-dimensional contour plot of reflection loss is included in the supplementary information (Fig. S2).

The attenuation constant (α) quantifies the material's overall attenuation capacity due to dielectric and magnetic losses. It can be expressed as [101].

$$\alpha = \frac{\sqrt{2}\pi f}{c} \sqrt{(\mu''\varepsilon'' - \mu'\varepsilon') + \sqrt{(\mu''\varepsilon'' - \mu'\varepsilon')^2 + (\varepsilon'\mu'' + \varepsilon''\mu')^2}} \tag{13}$$

The attenuation constant, a measure of the material's ability to attenuate electromagnetic waves, shows a positive correlation with frequency (Fig. 12a), reflecting the microwave absorption capability of the composite. The presence of graphite flakes and cobalt ferrite nanoparticles synergistically led to the beneficial attenuation constant of the CEM-GF-CF nanocomposite, particularly at

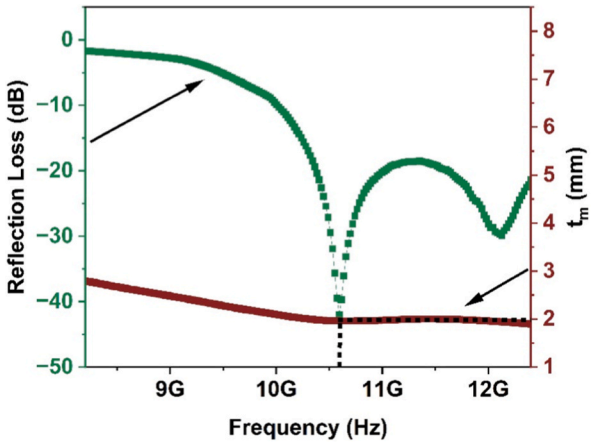

Fig. 11. Quarter-wave matching thickness (t_m) alongside the RL plot of CEM-GF-CF nanocomposites over frequency.

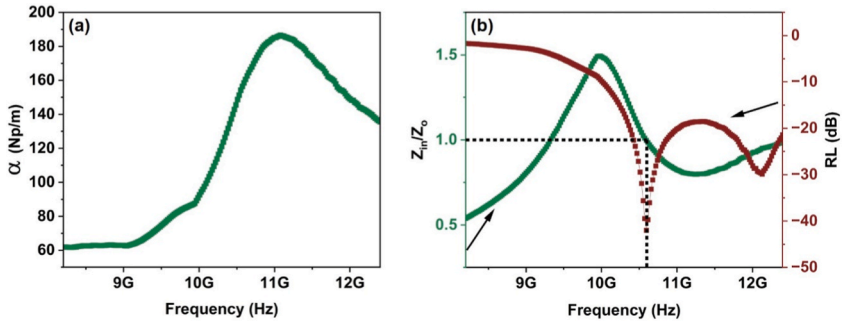

Fig. 12. (a) attenuation constant, and **(b)** impedance matching coefficient, alongside the RL plot of CEM-GF-CF nanocomposites over frequency.

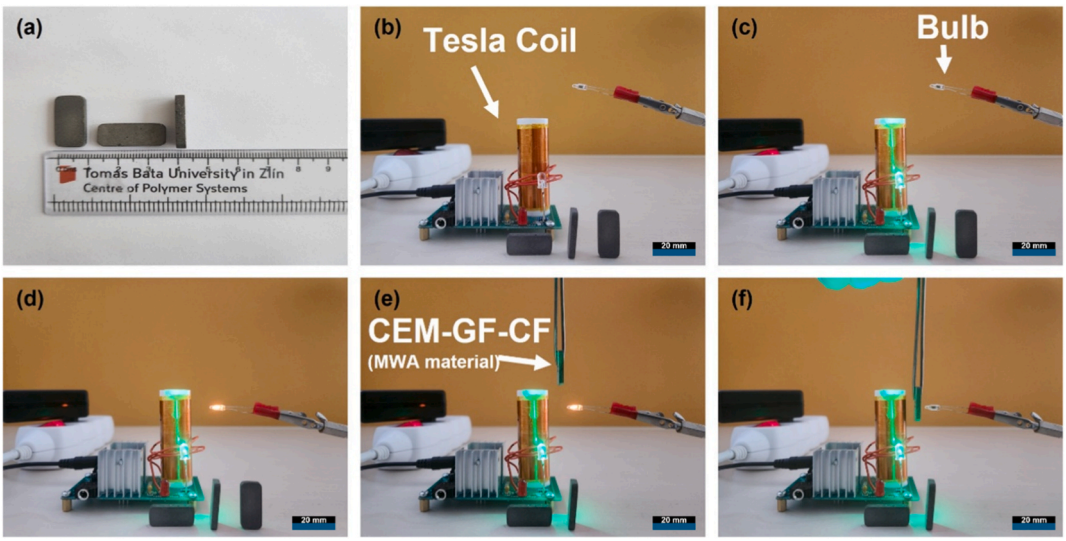

Fig. 13. Simple demonstration of electromagnetic wave absorption performance. **(a)** prepared 2 mm CEM-CF-GF nanocomposite, **(b)** setup with tesla transformer coil and light bulb (no power), **(c)** coil energized, but bulb remains off when positioned at a distance, **(d)** bulb glows when brought near the energized coil due to electromagnetic field coupling, **(e)** setup before sample insertion, **(f)** bulb intensity suppressed when the sample is introduced between the coil and bulb.

frequencies where both dielectric and magnetic losses are maximized. The obtained attenuation constant value leads to a greater reduction in the reflected microwave, as confirmed by the lower reflection loss values at these frequencies.

Impedance matching is a crucial factor for designing efficient microwave absorbers, with the goal of achieving minimal reflection (high absorption) across a broad frequency range. The impedance matching coefficient (Z), defined as the ratio between the input impedance of the composite material (Z_{in}) and that of free space (Z_0), determines the extent to which microwave waves are transmitted into the material rather than being reflected at the surface. The impedance matching coefficient can be calculated by using the following mathematical expressions [102–104]

$$Z = Z_{in}/Z_o \tag{14}$$

$$Z_{in} = Z_o\sqrt{\frac{\mu_r}{\varepsilon_r}}\tanh\left[j\left(\frac{2\pi fd}{c}\right)\sqrt{\mu_r\varepsilon_r}\right]$$

Fig. 12b depicts the impedance matching coefficient (Z_{in}/Z_o) over the same frequency range. For efficient impedance matching with free space ($Z_o = 377\ \Omega$), Z_{in}/Z_o should ideally approach 1. In this case, approximately at 10.6 GHz, the impedance curve intersects the ideal line ($Z_{in}/Z_o \approx 1$), indicating near-perfect impedance matching [105–107]. Furthermore, three-dimensional contour plot of impedance matching is included in the supplementary information (Fig. S3). The RL minimum observed at around 10.6 GHz can thus be attributed to the synergistic effect of both quarter-wavelength and impedance matching mechanisms. This enhanced microwave absorption behavior of CEM-CF-GF nanocomposite at 2 mm was achieved through the synergistic effects of enhanced permittivity and permeability, attenuation constant, and impedance matching coefficient due to the incorporation of graphite flakes and cobalt ferrite nanoparticles in the cement matrix.

A simple experimental demonstration was performed to visualize the electromagnetic wave absorption behaviour of the prepared composite (Fig. 13). A Tesla transformer coil was used as the source of high-frequency electromagnetic fields, while a light bulb placed nearby acted as a field detector through electromagnetic coupling. When the bulb was positioned close to the energized coil, it lit up due to strong field interaction. However, upon introducing the composite sample between the coil and the bulb, the light intensity was significantly suppressed, indicating that the sample effectively attenuates the incident electromagnetic field. This qualitative test illustrates the microwave absorption capability of the material in a clear and intuitive manner.

The effective microwave absorption of the cement-based $CoFe_2O_4$-graphite (CEM-CF-GF) composite arises from a synergy of dielectric and magnetic loss mechanisms, supported by its fillers and multiple heterogeneous phases (Fig. 14). Upon exposure to incident microwaves, part of the wave is reflected. At the same time, the rest penetrates the material due to favourable impedance matching with free space (Fig. 12b). Once inside, the energy is dissipated through several simultaneous processes. Dielectric losses dominate due to conduction loss via the graphite flakes, enabling electron mobility and electromagnetic energy conversion into heat [13,108]. Simultaneously, electron hopping within the $CoFe_2O_4$ lattice contributes additional dielectric dissipation through charge transport between multivalent ions [109]. Interfaces formed between the fillers and cement phases give rise to interfacial polarization, where trapped charges respond to the alternating field, generating localized dipoles [33]. Polar functional groups and intrinsic defects contribute to dipole polarization, further enhancing energy loss through continuous realignment of charges under microwave exposure [110]. Magnetic $CoFe_2O_4$ nanoparticles exhibit natural resonance in the applied frequency range on the magnetic front, promoting magnetic energy absorption [111]. Additionally, eddy currents induced in the nanocomposite generate resistive heating, aiding overall energy dissipation [112]. The complex, multiple heterogeneous microstructures promote internal scattering and multiple reflections,

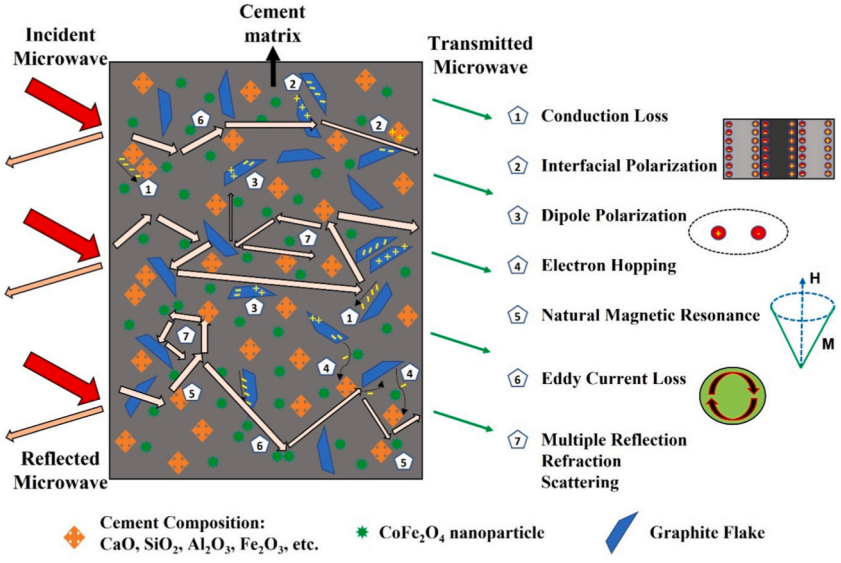

Fig. 14. Schematic representation of the microwave absorption mechanism that occurs in the developed CEM-CF-GF nanocomposite.

extending the wave path and maximizing absorption probability [33]. Together, these mechanisms ensure strong microwave absorption performance, validating the potential of the CEM-CF-GF composite as an efficient absorber material.

4. Conclusion

This study demonstrates that incorporating conductive graphite flakes (GF, 2.5 wt%) and magnetic $CoFe_2O_4$ (CF, 7.5 wt%) into a cement matrix can produce a cementitious absorber with excellent X-band microwave attenuation. The combined role of dielectric and magnetic fillers provides a balanced loss mechanism and ensures that impedance matching is achieved, enabling efficient absorption of incident microwaves. The following conclusion can be drawn.

1. The CEM-CF-GF composite with 2 mm thickness achieved a minimum reflection loss of −41.9 dB at 10.59 GHz with an effective absorption bandwidth of 2.4 GHz (10.0-12.4 GHz, RL < −10 dB), corresponding to microwave absorption efficiency of 99.994%.
2. The strong absorption performance arises from the synergetic interplay of dielectric and magnetic losses. Graphite flakes contribute conduction pathways and dielectric loss, while $CoFe_2O_4$ introduces magnetic loss mechanisms such as natural resonance and eddy-current effects. Additionally, interfacial polarization between fillers and the cement matrix, along with multiple scattering from heterogeneous filler domains, enhance energy dissipation across the X-band. The combined effect of these mechanisms ensures wide bandwidth and high attenuation efficiency.
3. A simple coil–bulb experiment qualitatively confirmed the EM wave absorption capability of the composites, showing suppression of electromagnetic field coupling when the sample was introduced between the source and detector. This practical demonstration aligns with the quantitative reflection loss and impedance results. Future studies should focus on expanding measurements to higher frequency ranges and exploring multilayer or hybrid composite designs.
4. Based on its strong microwave absorption within the X-band (8.2–12.4 GHz), the developed CEM-CF-GF composite shows promise for practical construction-based microwave absorption applications. Potential use cases include radar-absorbing building facades, secure facility walls, anechoic chamber linings, and protective enclosures for sensitive medical or laboratory equipment requiring mitigation of external RF interference.

CRediT authorship contribution statement

Vanamoorthy Mariappan: Writing – original draft, Software, Investigation, Formal analysis, Data curation. **Eliška Křivánková:** Formal analysis, Data curation. **Milan Masař:** Formal analysis, Data curation. **Marek Jurča:** Formal analysis, Data curation. **Michal Machovský:** Formal analysis, Data curation. **Lukáš Kalina:** Formal analysis, Data curation. **Jarmila Vilčáková:** Visualization, Formal analysis, Data curation. **Ivo Kuřitka:** Visualization, Project administration, Funding acquisition. **Martin Boháč:** Validation, Supervision, Conceptualization. **Raghvendra Singh Yadav:** Writing – review & editing, Supervision, Project administration, Investigation, Funding acquisition, Conceptualization.

Declaration of competing interest

The authors declare that they have no known competing financial interests or personal relationships that could have appeared to influence the work reported in this paper.

Acknowledgments

This work was financially supported by the Ministry of Education, Youth, and Sports of the Czech Republic-DKRVO (RP/CPS/2024-28/007) at the Centre of Polymer Systems, Tomas Bata University in Zlin, Czech Republic. One author, Vanamoorthy Mariappan, acknowledges the financial support provided by the Internal Grant Agency (IGA/CPS/2025/004).

Appendix A. Supplementary data

Supplementary data to this article can be found online at https://doi.org/10.1016/j.jobe.2026.115725.

Data availability

Data will be made available on request.

References

[1] N. Jayaraju, M. Pramod Kumar, G. Sreenivasulu, T. Lakshmi Prasad, B. Lakshmanna, K. Nagalaksmi, M. Madakka, Mobile phone and base stations radiation and its effects on human health and environment, A review, Sustainable Technology and Entrepreneurship 2 (2023), https://doi.org/10.1016/j.stae.2022.100031.

[2] A. Sharma, A review on the health implications of electromagnetic radiations emitting from cell phone towers, Annu Res Rev Biol 39 (2024) 87–93, https://doi.org/10.9734/arrb/2024/v39i62091.

[3] S. Sivani, D. Sudarsanam, Impacts of radio-frequency electromagnetic field (RF-EMF) from cell phone towers and wireless devices on biosystem and ecosystem-a review biology and Medicine impacts of radio-frequency electromagnetic field (RF-EMF) from cell phone towers and wireless devices on biosystem and ecosystem-a review. www.biolmedonline.com, 2012.

[4] Y. Wu, Y. Wang, X. Liu, G. Ma, Effects of layered and metasurface structures on the electromagnetic wave absorption performance of cementitious materials, J. Build. Eng. 72 (2023), https://doi.org/10.1016/j.jobe.2023.106719.

[5] K. Cui, J. Chang, L. Feo, C.L. Chow, D. Lau, Developments and applications of carbon nanotube reinforced cement-based composites as functional building materials, Front. Mater. 9 (2022), https://doi.org/10.3389/fmats.2022.861646.

[6] X. Jiang, D. Lu, B. Yin, Z. Leng, Advancing carbon nanomaterials-engineered self-sensing cement composites for structural health monitoring: a state-of-the-art review, J. Build. Eng. 87 (2024), https://doi.org/10.1016/j.jobe.2024.109129.

[7] W. Li, W. Dong, Y. Guo, K. Wang, S.P. Shah, Advances in multifunctional cementitious composites with conductive carbon nanomaterials for smart infrastructure, Cem. Concr. Compos. 128 (2022), https://doi.org/10.1016/j.cemconcomp.2022.104454.

[8] H. Qin, S. Ding, A. Ashour, Q. Zheng, B. Han, Revolutionizing infrastructure: the evolving landscape of electricity-based multifunctional concrete from concept to practice, Prog. Mater. Sci. 145 (2024), https://doi.org/10.1016/j.pmatsci.2024.101310.

[9] A.K. Thomoglou, M.G. Falara, M.E. Voutetaki, J.G. Fantidis, B.A. Tayeh, C.E. Chalioris, Electromechanical properties of multi-reinforced self-sensing cement-based mortar with MWCNTs, CFs, and PPs, Constr. Build. Mater. 400 (2023), https://doi.org/10.1016/j.conbuildmat.2023.132566.

[10] S. Zhai, B. Pang, G. Liu, Y. Zhang, K. Xu, W. She, Y. Zhang, Investigation on preparation and multifunctionality of reduced graphene oxide cement mortar, Constr. Build. Mater. 275 (2021), https://doi.org/10.1016/j.conbuildmat.2020.122119.

[11] W. Li, X. Li, S.J. Chen, Y.M. Liu, W.H. Duan, S.P. Shah, Effects of graphene oxide on early-age hydration and electrical resistivity of Portland cement paste, Constr. Build. Mater. 136 (2017) 506–514, https://doi.org/10.1016/j.conbuildmat.2017.01.066.

[12] F. Maria, T. Athanasia, G. Fani, E. Anaxagoras, Carbon nanotubes' amount and type: crucial parameters in mechanical performance enhancement on cement paste nanocomposites, J Phys Conf Ser, Institute of Physics (2022), https://doi.org/10.1088/1742-6596/2321/1/012003.

[13] D.D.L. Chung, A review of microwave absorption and reflection by cement-based materials, with emphasis on electromagnetic interference shielding and admixture effects, Adv. Funct. Mater. (2024), https://doi.org/10.1002/adfm.202408220.

[14] S. Dias, J. Almeida, A. Tadeu, J. de Brito, Alternative concrete aggregates - review of physical and mechanical properties and successful applications, Cem. Concr. Compos. (2024) 105663, https://doi.org/10.1016/j.cemconcomp.2024.105663.

[15] L. Musil, R. Chylik, J. Vodicka, The effect of granite filler on the rheological properties of fresh mixture of cement composites, J Phys Conf Ser, Institute of Physics (2022), https://doi.org/10.1088/1742-6596/2341/1/012014.

[16] Y. Dai, J. Wu, F. Wang, N. Zhu, H. Tang, Z. Zhang, Research on electromagnetic wave absorption properties of Portland cement, Mater. Res. Bull. 178 (2024), https://doi.org/10.1016/j.materresbull.2024.112903.

[17] Y. Wang, X. Li, J. Wei, Y. Zhang, Z. Miao, Z. Jia, Broadband electromagnetic wave absorption properties of RGO cement-based composite, Fullerenes, Nanotub. Carbon Nanostruct. 32 (2024) 936–942, https://doi.org/10.1080/1536383X.2024.2349766.

[18] X. Liu, Y. Zhang, Y. Guo, X. Wang, Optimization of electromagnetic wave absorption performance for magnesium phosphate cement using Fe3O4@SiO2 nanoparticles, Constr. Build. Mater. 435 (2024), https://doi.org/10.1016/j.conbuildmat.2024.136796.

[19] J. Xie, K. Li, Y. Zhang, M. Xiao, H. Guan, D. Wang, L. Yang, Electromagnetic absorption properties of composite mortar with graphene and manganese-zinc ferrite, J. Build. Eng. 97 (2024), https://doi.org/10.1016/j.jobe.2024.110963.

[20] Y. hua Bai, Y. jie Chen, Y. Lu, Graphite-enhanced foam cement-based materials: mechanical properties, pore structure and electromagnetic wave absorption performance, Mater. Today Commun. 40 (2024), https://doi.org/10.1016/j.mtcomm.2024.109377.

[21] Z. Chen, C. Zhang, Y. Zhu, J. Zou, Y. Chen, Enhanced electromagnetic wave absorption in ultrathin cement-based composites with integrated multi-dimensional carbon materials, Constr. Build. Mater. 432 (2024), https://doi.org/10.1016/j.conbuildmat.2024.136595.

[22] Z. Wu, S. Xie, Z. Ji, C. Ma, T. Si, J. Wu, J. Wang, Novel lightweight cement-based materials foaming by secondary aluminum ash: microwave absorption, mechanical and thermal insulation properties, Constr. Build. Mater. 413 (2024), https://doi.org/10.1016/j.conbuildmat.2023.134328.

[23] J. Ma, B. Zhao, H. Xiang, F.Z. Dai, Y. Liu, R. Zhang, Y. Zhou, High-entropy spinel ferrites MFe2O4 (M = Mg, Mn, Fe, Co, Ni, Cu, Zn) with tunable electromagnetic properties and strong microwave absorption, J. Adv. Ceram. 11 (2022) 754–768, https://doi.org/10.1007/s40145-022-0569-3.

[24] W.M. Abd El-Gawad, E.M. Eldesouki, W.A. Abd El-Ghany, Development of high performance microwave absorption modified epoxy coatings based on nano-ferrites, Sci. Rep. 14 (2024), https://doi.org/10.1038/s41598-024-55571-y.

[25] P. Kumar, P. Negi, A.K. Dixit, H.B. Baskey, S. Kumar, A.K. Mishra, A. Kumar, Superparamagnetic nanocubes of Co and Cu co-doped Mn-based ferrites as microwave absorbing material, Mater. Chem. Phys. 319 (2024), https://doi.org/10.1016/j.matchemphys.2024.129360.

[26] P.P. Mohapatra, H.K. Singh, P. Dobbidi, Advancements in electromagnetic microwave absorbers: ferrites and carbonaceous materials, Adv. Colloid Interface Sci. 337 (2025), https://doi.org/10.1016/j.cis.2024.103381.

[27] P.P. Mohapatra, M.T. Sebastian, H.K. Singh, P. Dobbidi, Magnetic composites: a comprehensive review of microwave absorption and shielding properties, J. Sci. Adv. Mater. Devices 10 (2025), https://doi.org/10.1016/j.jsamd.2025.100978.

[28] M. Montazeri, S.M. Masoudpanah, B. Aslibeiki, T. Sarkar, Electromagnetic properties of in-situ synthesized CoFe2O4/CoFe/Ti3C2 composite powders, J. Alloys Compd. 1033 (2025), https://doi.org/10.1016/j.jallcom.2025.181207.

[29] J. Cui, D. Zhao, F. Zhang, Q. Feng, X. Zhu, J. Zhou, Z. Liu, Preparation and wave-absorbing properties of OPCS@CoFe2O4 core–shell structured wave-absorbing materials with multiple loss mechanisms, J. Mater. Sci. Mater. Electron. 36 (2025), https://doi.org/10.1007/s10854-025-14563-y.

[30] Y. Zhang, S. Gao, X. Zhang, D. Ma, C. Zhu, J. He, Structural and microwave absorption properties of CoFe2O4/residual carbon composites, international journal of Minerals, Metallurgy and Materials 32 (2025) 221–232, https://doi.org/10.1007/s12613-024-2849-0.

[31] P. Anil, A. Joseph, B. Arun, K.C.J. Raju, V.V.R.K. Kumar, Enhanced X-band microwave absorption properties of cobalt ferrite/nitrogen-doped rGO nanocomposites, Mater. Sci. Eng., B 323 (2026), https://doi.org/10.1016/j.mseb.2025.118859.

[32] Q. Wang, X. Liu, J. Cui, Y. Yan, Gradient and flexible poly(vinylidene fluoride) composite with synergistically enhanced wave absorption performance by MXene and hollow cobalt ferrite, Chem. Eng. J. 520 (2025), https://doi.org/10.1016/j.cej.2025.165961.

[33] V. Mariappan, E. Křivánková, M. Masař, M. Machovský, J. Vilčáková, I. Kuřitka, M. Boháč, R.S. Yadav, Superior microwave absorbing cement-based composite using graphite flake/MnFe2O4 spinel ferrite nanoparticles, Constr. Build. Mater. 471 (2025), https://doi.org/10.1016/j.conbuildmat.2025.140600.

[34] G. Deng, Y. Yang, Q. Zhou, Y. Lei, L. Yue, T. Yang, Lightweight and broadband electromagnetic wave absorbing foamed cement-based composites incorporated with hybrid dielectric fibers, Constr. Build. Mater. 327 (2022), https://doi.org/10.1016/j.conbuildmat.2022.126931.

[35] L. Liang, Q. Li, X. Yan, Y. Feng, Y. Wang, H. Bin Zhang, X. Zhou, C. Liu, C. Shen, X. Xie, Multifunctional magnetic Ti3C2TxMXene/Graphene aerogel with superior electromagnetic wave absorption performance, ACS Nano 15 (2021) 6622–6632, https://doi.org/10.1021/acsnano.0c09982.

[36] D. Skoda, J. Vilcakova, R.S. Yadav, B. Hanulikova, T. Capkova, M. Jurca, M. Urbanek, P. Machac, L. Simonikova, J. Antos, I. Kuritka, Nickel nanoparticle–decorated reduced graphene oxide via one-step microwave-assisted synthesis and its lightweight and flexible composite with polystyrene-block-poly(ethylene-ran-butylene)-block-polystyrene polymer for electromagnetic wave shielding application, Adv. Compos. Hybrid Mater. 6 (2023), https://doi.org/10.1007/s42114-023-00692-7.

[37] B. Guan, D. Ding, L. Wang, J. Wu, R. Xiong, The electromagnetic wave absorbing properties of cement-based composites using natural magnetite powders as absorber, Mater. Res. Express 4 (2017), https://doi.org/10.1088/2053-1591/aa7025.

[38] Y. Ren, X. Wang, J. Ma, Q. Zheng, L. Wang, W. Jiang, Metal-organic framework-derived carbon-based composites for electromagnetic wave absorption: dimension design and morphology regulation, J. Mater. Sci. Technol. 132 (2023) 223–251, https://doi.org/10.1016/j.jmst.2022.06.013.

[39] H.M. Albetran, Structural characterization of graphite nanoplatelets synthesized from graphite flakes. https://doi.org/10.20944/preprints202008.0325.v1, 2020.

[40] Q.T. Ain, S.H. Haq, A. Alshammari, M.A. Al-Mutlaq, M.N. Anjum, The systemic effect of PEG-nGO-induced oxidative stress in vivo in a rodent model, Beilstein J. Nanotechnol. 10 (2019) 901–911, https://doi.org/10.3762/bjnano.10.91.

[41] M. Fu, Q. Jiao, Y. Zhao, H. Li, Vapor diffusion synthesis of CoFe2O4 hollow sphere/graphene composites as absorbing materials, J Mater Chem A Mater 2 (2014) 735–744, https://doi.org/10.1039/c3ta14050d.

[42] R. Prakshale, S. Bangale, M. Kamble, S. Sonawale, Synthesis, study and characterization of spinel CoFe2O4 for the ethanol gas-sensing applications, J. Mater. Sci. Mater. Electron. 34 (2023), https://doi.org/10.1007/s10854-023-11253-5.

[43] K. Dubey, S. Dubey, V. Sahu, R.A. Parry, A. Modi, N.K. Gaur, Structural, optical and magnetic properties of CoFe2O4 nanoparticle synthesized by ultrasonication-assisted sol–gel technique, Appl. Phys. A Mater. Sci. Process. 128 (2022), https://doi.org/10.1007/s00339-022-05681-z.

[44] K. Wei, H.X. Huai, B. Zhao, J. Zheng, G.Q. Gao, X.Y. Zheng, C.C. Wang, Facile synthesis of CoFe2O4 nanoparticles and their gas sensing properties, Sens. Actuators, B Chem. 369 (2022), https://doi.org/10.1016/j.snb.2022.132279.

[45] M. Szeląg, Influence of specimen's shape and size on the thermal cracks' geometry of cement paste, Constr. Build. Mater. 189 (2018) 1155–1172, https://doi.org/10.1016/j.conbuildmat.2018.09.078.

[46] M. Grzegorczyk-Frańczak, D. Barnat-Hunek, K. Materak, G. Łagód, Influence of water with oxygen and ozone micro-nano bubbles on concrete physical properties, Materials 15 (2022), https://doi.org/10.3390/ma15227938.

[47] M.A. Hassaan, A.I. Meky, H.A. Fetouh, A.M. Ismail, A. El Nemr, Central composite design and mechanism of antibiotic ciprofloxacin photodegradation under visible light by green hydrothermal synthesized cobalt-doped zinc oxide nanoparticles, Sci. Rep. 14 (2024), https://doi.org/10.1038/s41598-024-58961-4.

[48] A. Tun Naziba, M. Tun Nafisa, R. Sultana, M. Fahim Ehsan, A.R.M. Tareq, R. Rashid, H. Das, A.K.M. Atique Ullah, A.K.M. Fazle Kibria, Structural, optical, and magnetic properties of Co-doped ZnO nanorods: advancements in room temperature ferromagnetic behavior for spintronic applications, J. Magn. Magn Mater. 593 (2024), https://doi.org/10.1016/j.jmmm.2024.171836.

[49] M. Priyanka, G.S. Reddy, T.R. Kumar Reddy, C.S. Naveen, C.N.S. Kumar, M. Lodhe, B.K. Kodli, C.S. Ramesh, Synthesis and characterization of Y and Mn -doped ZnO nanoparticles: structural, optical, morphological, and gas sensing investigations, Phys. B Condens. Matter 687 (2024), https://doi.org/10.1016/j.physb.2024.416109.

[50] B. Unveroglu Abdioglu, Structure and morphology modification of ZnO nanocrystals via substitutional cobalt doping for enhanced electrochemical activity, Phys. B Condens. Matter 684 (2024), https://doi.org/10.1016/j.physb.2024.415968.

[51] M.I. Arshad, M.S. Hasan, A.U. Rehman, M. Akhtar, L.D. Tung, N. Amin, K. Mahmood, A. Ali, T. Trakoolwilaiwan, N.T.K. Thanh, Structural, optical, electrical, dielectric, molecular vibrational and magnetic properties of La3+ doped mg–cd–cu ferrites prepared by Co-precipitation technique, Ceram. Int. 48 (2022) 14246–14260, https://doi.org/10.1016/j.ceramint.2022.01.313.

[52] M.A. Darwish, M.M. Hussein, S.A. Saafan, W. Abd-Elaziem, D. Zhou, M.V. Silibin, S.V. Trukhanov, N.V. Abmiotka, M.I. Sayyed, D.I. Tishkevich, A. V. Trukhanov, Impact of the Mg/Zn ratio on features of structural and magnetic properties in A-site stoichiometric nanosized spinel ferrites, J. Alloys Compd. 968 (2023), https://doi.org/10.1016/j.jallcom.2023.172278.

[53] M.S. Hasan, S.S. Ali, M.I. Khan, M. Rizwan, M. Zulqarnain, A. Hussain, Structural, optical, electrical and magnetic tuning based on Zn substitution at A site in yttrium doped spinel ferrites, Mater. Chem. Phys. 301 (2023), https://doi.org/10.1016/j.matchemphys.2023.127538.

[54] W. Zhou, Q. Ye, Z. Zhou, X. Sun, J. Zhang, J. Cao, J. Li, Green and efficient production of functionalized graphite reinforced magnesium oxychloride cement-based materials, Constr. Build. Mater. 417 (2024), https://doi.org/10.1016/j.conbuildmat.2024.135320.

[55] E. Wieland, G.D. Miron, B. Ma, G. Geng, B. Lothenbach, Speciation of iron(II/III) at the iron-cement interface: a review, Materials and Structures/Materiaux et Constructions 56. https://doi.org/10.1617/s11527-023-02115-x, 2023.

[56] S. Hunpratub, S. Phokha, P. Kidkhunthod, N. Chanlek, P. Chindaprasirt, The effect of cation distribution on the magnetic properties of CoFe2O4 nanoparticles, Results Phys. 24 (2021), https://doi.org/10.1016/j.rinp.2021.104112.

[57] R.J. Pan, J. Wu, J. Qu, T. Zhang, F.Z. Jiao, M. Zhao, M.Y. Han, X. Li, Z.Z. Yu, Peak-like three-dimensional CoFe2O4/carbon nanotube decorated bamboo fabrics for simultaneous solar-thermal evaporation of water and photocatalytic degradation of bisphenol A, J. Mater. Sci. Technol. 179 (2024) 40–49, https://doi.org/10.1016/j.jmst.2023.08.045.

[58] H. Zhang, Y. Zhao, X. Zuo, H. Huang, C. Sun, Z. Fan, L. Pan, Construction of chiral-magnetic-dielectric trinity composites for efficient microwave absorption with low filling ratio and thin thickness, Chem. Eng. J. 467 (2023), https://doi.org/10.1016/j.cej.2023.143414.

[59] G.C. Lavorato, M.E. Saleta, S.J.A. Figueroa, D. Tobia, J.C. Mauricio, J. Lohr, E. Baggio-Saitovitch, H.E. Troiani, R.D. Zysler, E. Lima, E.L. Winkler, Cation occupancy in bimagnetic CoO-core/Co1−xZnxFe2O4-shell (x = 0-1) nanoparticles, J. Alloys Compd. 877 (2021), https://doi.org/10.1016/j.jallcom.2021.160172.

[60] D. Carta, C. Marras, D. Loche, G. Mountjoy, S.I. Ahmed, A. Corrias, An X-ray absorption spectroscopy study of the inversion degree in zinc ferrite nanocrystals dispersed on a highly porous silica aerogel matrix, J. Chem. Phys. 138 (2013), https://doi.org/10.1063/1.4789479.

[61] Q. Wei, L. Xu, Z. Tang, Z. Xu, C. Xie, L. Guo, W. Li, High-performance expanded graphite from flake graphite by microwave-assisted chemical intercalation process, J. Ind. Eng. Chem. 122 (2023) 562–572, https://doi.org/10.1016/j.jiec.2023.03.020.

[62] L. Huang, G. Xiao, Y. Wang, H. Li, Y. Zhou, L. Jiang, J. Wang, Self-exfoliation of flake graphite for bioinspired compositing with aramid nanofiber toward integration of mechanical and thermoconductive properties, Nano-Micro Lett. 14 (2022), https://doi.org/10.1007/s40820-022-00919-0.

[63] Česká Agentura Pro Standardizaci S.P.O. ČSN EN 196 – Metody Zkoušení Cementu. 10/2016. TECHNOR print s r o., in: n.d.

[64] Česká Agentura Pro Standardizaci S.P.O. ČSN EN 197-1 ED.2 – Cement - Část 1: Složení, Specifikace a Kritéria Shody Cementů Pro Obecné Použití. 04/2012. Technor Print S R O., (n.d.).

[65] M. Ren, F. Li, P. Gao, Y. Niu, J. Wei, Q. Yu, Design and preparation of double-layer structured cement-based composite with inspiring microwave absorbing property, Constr. Build. Mater. 263 (2020), https://doi.org/10.1016/j.conbuildmat.2020.120670.

[66] Y. hua Bai, D. yue Zhang, Y. Lu, Foamed concrete composites: Mn–Zn ferrite/carbon fiber synergy enhances electromagnetic wave absorption performance, Ceram. Int. 49 (2023) 33703–33716, https://doi.org/10.1016/j.ceramint.2023.08.058.

[67] Y. Dai, M. Sun, C. Liu, Z. Li, Electromagnetic wave absorbing characteristics of carbon black cement-based composites, Cem. Concr. Compos. 32 (2010) 508–513, https://doi.org/10.1016/j.cemconcomp.2010.03.009.

[68] J. Liang, F. Ye, Q. Song, Y. Cao, S. Hui, Y. Qin, H. Wu, In-Plane heterogeneous structure-boosted interfacial polarization in graphene for wide-band and wide-temperature microwave absorption, Chem. Eng. J. 497 (2024), https://doi.org/10.1016/j.cej.2024.154307.

[69] L. Ren, Y. Wang, X. Zhang, Q. He, G. Wu, Efficient microwave absorption achieved through in situ construction of core-shell CoFe2O4@mesoporous carbon hollow spheres, Int. J. Min. Met. Mater. 30 (2023) 504–514, https://doi.org/10.1007/s12613-022-2509-1.

[70] R. Song, Y. Si, W. Qian, H. Zu, B. Zhou, Q. Du, D. He, Y. Wang, Investigation of MXene nanosheets based radio-frequency electronics by skin depth effect, Nano Res. 17 (2024) 3061–3067, https://doi.org/10.1007/s12274-023-6127-7.

[71] W. Zhou, C. Jiang, X. Duan, J. Song, Y. Yuan, N. Chen, Fe3O4/carbonized cellulose micro-nano hybrid for high-performance microwave absorber, Carbohydr. Polym. 245 (2020), https://doi.org/10.1016/j.carbpol.2020.116531.

[72] A. Gorai, A. Dutta, K. Mandal, Enhancement of microwave absorption properties of crystal-engineered perovskite oxide using cobalt ferrite, Adv. Eng. Mater. (2024), https://doi.org/10.1002/adem.202401173.

[73] Z. Yang, Y. Yao, Y. Zhuge, Enhancing electromagnetic shielding performance of cement-based materials using industrial waste copper swarf, Constr. Build. Mater. 426 (2024), https://doi.org/10.1016/j.conbuildmat.2024.136162.

[74] I.W. Nam, H.K. Lee, Synergistic effect of MWNT/fly ash incorporation on the EMI shielding/absorbing characteristics of cementitious materials, Constr. Build. Mater. 115 (2016) 651–661, https://doi.org/10.1016/j.conbuildmat.2016.04.082.

[75] L. Wang, X. Li, X. Shi, M. Huang, X. Li, Q. Zeng, R. Che, Recent progress of microwave absorption microspheres by magnetic-dielectric synergy, Nanoscale 13 (2021) 2136–2156, https://doi.org/10.1039/d0nr06267g.

[76] A.L. Sharma, A.K. Thakur, AC conductivity and relaxation behavior in ion conducting polymer nanocomposite, Ionics 17 (2011) 135–143, https://doi.org/10.1007/s11581-010-0502-6.

[77] A. Chandra Anjana, Facile synthesis and characterization of polymer composites with cobalt ferrite and biomass based activated carbon for microwave absorption, Mater. Today Commun. 37 (2023), https://doi.org/10.1016/j.mtcomm.2023.107397.

[78] C. Guo, C. Chen, R. Wan, L. Yang, Y. Guan, P. Wang, Iodide-based glass with combination of high transparency and conductivity: a novel promising candidate for transparent microwave absorption and radar stealth, Chem. Eng. J. 484 (2024), https://doi.org/10.1016/j.cej.2024.148930.

[79] Y.N. Shen, Y.H. Fang, D.D. Zhang, B. Wang, F.Y. Zhuo, B.T. Huang, Microwave absorption and electromagnetic properties of ultra-high-strength cementitious materials: influence of basalt powder and underlying mechanism, Constr. Build. Mater. 432 (2024), https://doi.org/10.1016/j.conbuildmat.2024.136639.

[80] Y. Wu, X. Liu, Y. Xu, B. Liu, Enhanced electromagnetic wave absorption performance in the S-band with reconfigurable encoding phase gradient metasurface of cementitious materials, J. Build. Eng. 112 (2025), https://doi.org/10.1016/j.jobe.2025.113850.

[81] C. Srinivas, K. Naga Praveen, E. Ranjith Kumar, T.V. Chandrasekhar Rao, C.L. Prajapat, S.S. Meena, P. Bhatt, B. Arun, K.C. James Raju, D.L. Sastry, Shielding performance of MnxNi0.8–xZn0.2Fe2O4 (0.1≤x≤0.7) for electromagnetic interference (EMI) in X-band frequency, Ceram. Int. 48 (2022) 9987–9997, https://doi.org/10.1016/j.ceramint.2021.12.205.

[82] N. Anju, M. Masař, M. Machovský, M. Urbánek, P. Šuly, B. Hanulíková, J. Vilčáková, I. Kuřitka, R.S. Yadav, Optimization of CoFe2O4 nanoparticles and graphite fillers to endow thermoplastic polyurethane nanocomposites with superior electromagnetic interference shielding performance, Nanoscale Adv. 6 (2024) 2149–2165, https://doi.org/10.1039/d3na01053h.

[83] T. Govindasamy, N.K. Mathew, V.K. Asapu, V. Subramanian, B. Subramanian, Modulating the structural and magnetic properties of Fe3O4 NPs for high-performance supercapattery and EMI shielding applications, J. Energy Storage 79 (2024), https://doi.org/10.1016/j.est.2023.110243.

[84] W. Wang, J. Wen, X. Hou, Y. Zhang, W. Ye, S. Wang, R. Zhao, W. Xue, Enhanced microwave absorption of superlattice C-CuS/MXene composites with rich heterogeneous interfaces and conductive network synergies, Mater. Today Phys. 35 (2023), https://doi.org/10.1016/j.mtphys.2023.101108.

[85] L. Ma, Y. Wu, Z. Wu, P. Xia, Y. He, L. Zhang, H. Fan, C. Tong, L. Zhang, X. Gao, L. Deng, Enhanced dielectric loss in N-doped three-dimensional porous carbon for microwave absorption, Mater Today Adv 20 (2023), https://doi.org/10.1016/j.mtadv.2023.100434.

[86] X. Liu, Y. Wang, Y. Zhang, Optimization of electromagnetic wave absorption performance for cementitious material with porous and functional multilayer structures design, J. Build. Eng. 112 (2025), https://doi.org/10.1016/j.jobe.2025.113814.

[87] X. Huang, M. Qiao, X. Lu, Y. Li, Y. Ma, B. Kang, B. Quan, G. Ji, Evolution of dielectric loss-dominated electromagnetic patterns in magnetic absorbers for enhanced microwave absorption performances, Nano Res. 14 (2021) 4006–4013, https://doi.org/10.1007/s12274-021-3327-x.

[88] H. Wei, Z. Zhang, G. Hussain, L. Zhou, Q. Li, K. (Ken) Ostrikov, Techniques to enhance magnetic permeability in microwave absorbing materials, Appl. Mater. Today 19 (2020), https://doi.org/10.1016/j.apmt.2020.100596.

[89] K.M. Batoo, M. Hadi, R. Verma, A. Chauhan, R. Kumar, M. Singh, O.M. Aldossary, Improved microwave absorption and EMI shielding properties of Ba-doped Co–Zn ferrite, Ceram. Int. 48 (2022) 3328–3343, https://doi.org/10.1016/j.ceramint.2021.10.108.

[90] C.J. Li, X. Wang, X. Liu, J. Zhang, S. Bi, Z.L. Hou, Broadband and strong microwave absorption combining excellent EMI shielding of VGCF/carbonyl iron composites derived from synergistic magnetic and dielectric losses, Carbon N Y 214 (2023), https://doi.org/10.1016/j.carbon.2023.118383.

[91] C. Zhou, X. Wang, H. Luo, L. Deng, S. Wei, Y. Zheng, Q. Jia, J. Liu, Rapid and direct growth of bipyramid TiO2 from Ti3C2Tx MXene to prepare Ni/TiO2/C heterogeneous composites for high-performance microwave absorption, Chem. Eng. J. 383 (2020), https://doi.org/10.1016/j.cej.2019.123095.

[92] N. Anju, M. Masař, M. Machovský, M. Urbánek, P. Šuly, B. Hanulíková, J. Vilčáková, I. Kuřitka, R.S. Yadav, Optimization of CoFe2O4 nanoparticles and graphite fillers to endow thermoplastic polyurethane nanocomposites with superior electromagnetic interference shielding performance, Nanoscale Adv. (2024), https://doi.org/10.1039/d3na01053h.

[93] A. Maryam, Z. Rizwan, N. Nasir, J. Ahmad, M. Imran khan, Y. Nawab, H. Shehbaz Ahmad, Optimization of percolation limit of carbon black for electromagnetic interference shielding, J. Magn. Magn Mater. 586 (2023), https://doi.org/10.1016/j.jmmm.2023.171164.

[94] X. Xi, M. Öztürk, J. Cai, L. Wang, Z. Zhao, H. Chu, Q. Ran, First study of quantitative relationship between electric polarization and electromagnetic interference (EMI) shielding effectiveness of CFRP, Carbon N Y 225 (2024), https://doi.org/10.1016/j.carbon.2024.119095.

[95] D.D.L. Chung, M. Ozturk, Electromagnetic skin depth of cement paste and its thickness dependence, J. Build. Eng. 52 (2022), https://doi.org/10.1016/j.jobe.2022.104393.

[96] D. Sahu, M.K. Panda, R. Panwar, Dielectric characterization of microwave absorbing and EMI shielding structures optimized through firefly algorithm, IEEE Trans. Dielectr. Electr. Insul. (2024), https://doi.org/10.1109/TDEI.2024.3414989.

[97] M. Green, A.T. Van Tran, X. Chen, Obtaining strong, broadband microwave absorption of polyaniline through data-driven materials discovery, Adv. Mater. Interfac. 7 (2020), https://doi.org/10.1002/admi.202000658.

[98] X. Yang, B. Lin, H. Wang, T. Zhu, J. Wei, C. Yang, P. Liu, B. Zhang, Q. Yu, L. Wang, Construction of heterostructured PAN@PDA@Ti 3 C 2 T x MXene composite films for enhanced microwave absorption performance, ACS Appl. Electron. Mater. (2024), https://doi.org/10.1021/acsaelm.4c01373.

[99] S. Zhang, M. Li, G. Chen, H. Wang, G. Shao, D. Lan, Y. Zhu, R. Zhang, L. Guan, B. Fan, Achieving high performance microwave attenuation by anchoring magnetic CoNi nanoparticles onto few-layer Ti3C2TxMXene, J. Alloys Compd. 1023 (2025), https://doi.org/10.1016/j.jallcom.2025.180015.

[100] K. Cao, X. Yang, Y. Zhang, J. Wen, J. Chen, X. Hou, R. Zhao, W. Xue, Preparation of magnetic three-dimensional porous Co-rGO aerogel for enhanced microwave absorption, Carbon N Y 208 (2023) 111–122, https://doi.org/10.1016/j.carbon.2023.03.037.

[101] R. Shu, W. Li, X. Zhou, D. Tian, G. Zhang, Y. Gan, J. Shi, J. He, Facile preparation and microwave absorption properties of RGO/MWCNTs/ZnFe2O4 hybrid nanocomposites, J. Alloys Compd. 743 (2018) 163–174, https://doi.org/10.1016/j.jallcom.2018.02.016.

[102] W. Hai, C. Chen, Q. Yu, M. Li, Z. Jiang, H. Shao, G. Shao, J. Jiang, N. Chen, S. Bi, Sandwich structure electromagnetic interference shielding composites based on Fe3O4 nanoparticles/PANI/laser-induced graphene with near-zero electromagnetic waves transmission, Appl. Surf. Sci. 637 (2023), https://doi.org/10.1016/j.apsusc.2023.157975.

[103] X. Zeng, X. Cheng, R. Yu, G.D. Stucky, Electromagnetic microwave absorption theory and recent achievements in microwave absorbers, Carbon N Y 168 (2020) 606–623, https://doi.org/10.1016/j.carbon.2020.07.028.

[104] R.S. Yadav, I. Kuřitka, Recent advances on outstanding microwave absorption and electromagnetic interference shielding nanocomposites of ZnO semiconductor, Adv. Colloid Interface Sci. 326 (2024), https://doi.org/10.1016/j.cis.2024.103137.

[105] B. Nazari, M. Ghahari, Z. Ranjbar, Synergistically enhanced electromagnetic absorption in barium ferrite/hollow carbon spheres/epoxy composites, Mater. Chem. Phys. 326 (2024), https://doi.org/10.1016/j.matchemphys.2024.129830.

[106] M. Bala, V.D. Shivling, S. Tyagi, Synergistic impact of nickel ferrite and titanium dioxide composites for improving microwave absorption in X-band, Mater. Sci. Eng., B 304 (2024), https://doi.org/10.1016/j.mseb.2024.117388.

[107] X. Bai, Y. Guo, H. Yan, J. Qi, H. Lu, Magnetic-dielectric synergistic construction of Ni-doped Ti3AlC2 achieving efficient microwave absorption, Ceram. Int. 49 (2023) 40570–40580, https://doi.org/10.1016/j.ceramint.2023.10.036.

[108] S. Sharma, S.R. Parne, S.S.S. Panda, S. Gandi, Progress in microwave absorbing materials: a critical review, Adv. Colloid Interface Sci. 327 (2024), https://doi.org/10.1016/j.cis.2024.103143.

[109] S.E. Shirsath, M.L. Mane, Y. Yasukawa, X. Liu, A. Morisako, Self-ignited high temperature synthesis and enhanced super-exchange interactions of Ho3+-Mn2+-Fe3+-O2- ferromagnetic nanoparticles, Phys. Chem. Chem. Phys. 16 (2014) 2347–2357, https://doi.org/10.1039/c3cp54257b.

[110] J. Wang, X. Sheng, S. Hao, G. Liu, R. Cai, X. Xue, Y. Wang, Construction of Fe0.64Ni0.36@graphite nanoparticles via corrosion-like transformation from NiFe2O4 and surface graphitization in flexible carbon nanofibers to achieve strong wideband microwave absorption, J. Colloid Interface Sci. 657 (2024) 193–207, https://doi.org/10.1016/j.jcis.2023.11.145.

[111] X.Y. Wang, S.Y. Liao, Y.J. Wan, P.L. Zhu, Y.G. Hu, T. Zhao, R. Sun, C.P. Wong, Electromagnetic interference shielding materials: recent progress, structure design, and future perspective, J Mater Chem C Mater 10 (2022) 44–72, https://doi.org/10.1039/d1tc04702g.

[112] F. Zhang, N. Li, J.F. Shi, L. Xu, L.C. Jia, Y.Y. Wang, D.X. Yan, Recent progress on carbon-based microwave absorption materials for multifunctional applications: a review, Compos. B Eng. 283 (2024), https://doi.org/10.1016/j.compositesb.2024.111646.